ADVANCED ENGINEERING MATERIALS

DOI: 10.1002/adem.201400078

Processing and Characterization of Aluminum Nitride Ceramics for High Thermal Conductivity**

By *Hyun Min Lee, Kamala Bharathi* and *Do Kyung Kim**

The effects of sintering additives, microstructure, and morphology of second phase on the thermal conductivity of aluminum nitride ceramics are discussed in this review. The thermal conductivity of AlN is highly dependent on the types and amount of sintering additives, second phase morphology and microstructure. The morphology of second phase in AlN ceramics could be controlled by changing the cooling rate. The amount of second phase was able to be minimized by using the transient sintering additives. The thermal conductivity of AlN could be enhanced with the inclusion of the transient sintering additives. The thermal conductivity of AlN ceramics was evaluated by Raman spectroscopy. High temperature AC impedance studies were conducted to characterize the electrical conduction mechanism of AlN ceramics.

1. Introduction

The ability of a material to conduct heat is called thermal conductivity.[1–4] Thermal conductivity in a solid can be expressed by the Fourier equation:[1–4] $dQ/dt = -kA\,(dt/dx)$, where dQ is the amount of heat flowing normal to the area A in time dt. Heat flow is proportional to the temperature gradient of dT/dx, and the proportionality factor k is material constant, which is thermal conductivity. An efficient conduction process (heating or cooling) is highly dependent on the thermal conductivity of the materials. In addition to the high thermal conductivity, material should have a low thermal expansion coefficient and low density to avoid heat dissipation and weight issues.[5] One challenging issue for the electronics and semiconductor industries to achieve high-performance devices with small size (miniaturization) is overcoming the heat dissipation problem.[5,6] The highest thermal conductivity values at room temperature can be found in diamonds or graphite (2000 $W\,m^{-1}\,K^{-1}$).[5] However, high cost and low quality make diamonds or other carbon-based materials unsuitable for industrial purposes. Among conducting materials, copper (Cu) is a very good thermal conductor, and at the same time, its thermal expansion is very large.[5,6] Materials having a low thermal expansion coefficient and light weight (i.e. aluminum) are preferable for the industrial applications.[5]

High thermal conductivity and a low thermal expansion coefficient can be achieved by preparing the composite material.[7] However, AlN has very high electrical resistivity, has a small thermal expansion coefficient, is nontoxic,[8–10] and importantly, is a very good phonon heat conductor, as predicted by Borom *et al*.[11] After the investigation of thermal conductivity of AlN by Slack *et al*.,[12], it has been an interesting topic to many research groups.[12–14] The thermal conductivity of pure AlN at room temperature has been predicted to be ≈320 $W\,m^{-1}\,K^{-1}$.[12–15] The important factors for any material to have high thermal conductivity are the following: (i) the strong bonding between the atoms, (ii) simple crystal structure with low atomic mass, and (iii) high purity and large Debye temperature (θD).[16]

[*] *D. K. Kim, H. M. Lee, K. Bharathi*
Department of Materials Science and Engineering, Korea Advanced Institute of Science and Technology (KAIST), 291 Daehak-ro, Yuseong-gu, Daejeon 305-701, Republic of Korea
E-mail: dkkim@kaist.ac.kr

[**] *This study was supported by a grant from the Fundamental R&D Program for Core Technology of Materials funded by the Ministry of Commerce, Industry and Energy, Republic of Korea. This work was also partially supported by Basic Science Research Program through the National Research Foundation of Korea (NRF) funded by the Ministry of Education (2009-0094038).*

REVIEW

In addition to the thermal conductivity properties, AlN has a large direct band gap of 6.2 eV, high refractive index (~2.0) and low-absorption coefficient ($<10^{-3}$).[17–20] Its excellent optical properties make it suitable for the development of optoelectronic devices operating near the short-wavelength end of the visible spectrum and high-frequency surface acoustic wave devices. These unique properties of AlN make it an excellent material to replace alumina (Al_2O_3) and berilia (BeO) used in the semiconductor industry.

Hyun Min Lee *graduated from Hongik University in South Korea with a degree in Material Science and Engineering and received his masters from KAIST (Korea Advanced Institute of Science and Technology) in Material Science and Engineering. He is working as a Ph.D candidate in Prof. Do Kyung Kim's group at KAIST, South Korea from Feb 2012. His research interest includes ceramic processing, sintering and characterization of nitride ceramics.*

Dr. Kamala Bharathi *received his masters (M.Sc.) from The American college, Madurai in India and Ph.D from IIT Madras, Chennai in India in 2010. He worked as a postdoctoral fellow in Prof. C.V. Ramana's group at UTEP, Texas, USA from 2010 March to 2011 May and Prof. Do Kyung Kim's group at KAIST, South Korea from June 2012 to Feb 2014. His research interest includes Magneto-electric materials, Multiferroic thin films, Rare earth doped Ni ferrite materials, Synthesis and characterization of nano-crystalline perovskite oxides, X-ray Phosphor materials, Li battery materials and their magnetic properties.*

Prof. Do Kyung Kim *joined the faculty of Department of Materials Science and Engineering, KAIST in 1994. He received his B.S. degree from Seoul National University in 1982 and earned M.S. and Ph.D. from Department of Materials Science and Engineering of KAIST in 1984 and 1987, respectively. Before joining KAIST, he worked for the Agency for Defense Development (1987–1994), Korea. He had spent several visiting professor positions in UC San Diego (1992), NIST (2002), and UC Berkeley (2008). He was awarded a Top 20 Most Outstanding Research Award from Korea Science and Engineering Foundation (KOSEF) in 1997 and Top Most Outstanding Research Award from Korea Research Foundation (KRF) in 2011. In 2007, he was awarded the Promising Scientist for Overseas Research by SBS Foundation. He has authored more than 150 technical articles, and has filled 17 Patents in US, Japan and Korea.*

AlN crystalizes in hexagonal 2H structure with the space group P63mc.[21] By incorporating sintering aids (Y, Ca, rare-earths, alkaline- earth oxides or mixture of oxides) into the hexagonal structure, AlN becomes a highly dense (3.260 g cm^{-3}) material.[22] The thermal conductivity of AlN is significantly affected by impurities or oxygen present in the sample. It has been reported that the oxygen atom replaces the nitrogen atom and dissolves in AlN grains and, subsequently, forms an Al vacancy. Phonon scattering caused by the Al vacancy leads to the reduction of thermal conductivity.[23,24]

By adding additives into the AlN matrix, the formation of a eutectic phase between the additive and the surface oxide layer leads to the prevention of the diffusion of oxygen into the grains by trapping it in the grain boundary.[23,24] The thermal conductivity of AlN can be enhanced by adding additive during sintering, but at the same time, the residual grain boundary phase affects the thermal conductivity of polycrystalline AlN. Therefore, it is very important to control the type and amount of additive added to the AlN matrix during the sintering process. In addition to the amount of additives, the morphology and microstructure of the second phase also greatly affect the thermal conductivity.

In the present paper, synthesis, structural, morphology, and thermal conductivity of highly pure AlN are reviewed. In addition to that, the effects of additives, second phase morphology, and microstructure on the thermal conductivity are also discussed. The AlN specimens with interconnected or isolated second phases were obtained by controlling the cooling rate after the sintering was carried out. The thermal conductivity of AlN specimens was theoretically calculated, and the results were compared with the experimentally measured values.

2. Processing

2.1. Sintering and Powder Processing

High density material can be achieved with starting materials as sub-micron powders or by applying very high pressure during the solid state sintering. Because of the highly covalent and low diffusive nature of AlN, sintering is a great challenging without any additives, and in order to achieve high density, the sintering must be carried out at very high temperatures (>1900 °C). As an alternative to high temperature/pressure sintering, Komeya *et al.*[25,26] have proposed adding alkaline-earth oxide or rare earth-oxide into AlN matrix can result in highly dense AlN during the sintering at ambient pressure.

Typically used commercial AlN powder (Grade E, Tokuyama Soda Co. Ltd., Tokyo) was employed for all the studies.[27–29] Table 1 shows the size and impurity content present in the sample. An average particle size of 1.0 μm was used for the studies. Twenty-four-hours ball-milling was carried out by mixing the AlN powders with isopropanol (IPA) as a liquid medium. After the milling, in order to

ADVANCED ENGINEERING MATERIALS 2014,
DOI: 10.1002/adem.201400078

ADVANCED ENGINEERING MATERIALS

Table 1. Physical properties and characteristics of the starting AlN powder.

Agglomerated particle size [μm]	Specific surface area [m^2g^{-1}]	Impurity contents				
		O	C	Ca	Si	Fe
1.0	3.5	0.85 wt%	370 ppm	8 ppm	<9 ppm	<10 ppm

evaporate the IPA, the slurry was dried in a hot-plate with magnetic stirring and dried completely in a vacuum oven at 60 °C.

The dried powder was pelletized into 20 mm diameter discs under a pressure of 30 kg cm^{-2} and followed by cold isostatic pressing at 200 MPa. The pellets were then sintered without applying any pressure at a temperature between 1700 and 1900 °C for 3 h in an N_2 atmosphere in a graphite resistance furnace (Astro Thermal Technology, Santa Barbara, CA).

2.2. Homogeneous Dispersion of Additives

Highly dense AlN can be achieved by adding the appropriate additives at ambient pressures. The thermal conductivity of AlN depends on several factors such as the physical and chemical homogeneity of AlN green compact, the amount and the type of additive used and the sintering conditions.[30–36] In addition to that, the thermal conductivity of AlN increases significantly with the addition of Y_2O_3. Y_2O_3 reacts with the surface oxide layers present in AlN powder, and yttrium aluminate liquid phase forms as a eutectic phase during the sintering (Figure 1),[37] which traps and prevents the diffusion of oxygen into AlN grain. The following properties are essential for the additives to be used for pressureless sintering: (i) chemical compatibility with the parent phase (AlN), which eliminates the possibilities of the formation of unwanted second phases, (ii) very high electrical resistivity to eliminate possible electrical short circuits through a small second phase segregated at grain boundaries, and (iii) in order to enhance the kinetics of densification, easy formation of liquid phase during the sintering. Y_2O_3 satisfies the above mentioned requirements, and it is one of the additives studied extensively by several research groups.[33,34] It has been reported that the mixing of Y_2O_3 ultra-fine particles (employing mechanical mixing) into an AlN matrix leads to enhancement of the thermal conductivity due to the fractionation of agglomeration.[33,34] However, chemical mixing has shown better homogenous mixing compared to the mechanical mixing. We have proposed a method of coating an Y_2O_3 precursor on the AlN powder by in situ precipitation in a non-aqueous system with minimization of the hydration of AlN powder.[27] Micron sized yttria (Y_2O_3, purity 99.99%, Alpa Products, Australia, primary particle size: 10 μm) and nano sized yttria (Y_2O_3, Aldrich, USA, primary particle size: 50 nm: specific surface area: 45 $m^2 g^{-1}$) were used as a sintering additive. In the case of yttria coating as sintering additive, AlN powder was dispersed in a calculated amount of yttrium nitrate (99.9%, Johnson Mattey Catalog Company, Ward Hill, MA) dissolved in isopropanol and coated using diethylamine (DEA, purity 99.0%, Junsei Chemical, Japan) as precipitating agent. After mixing the AlN powder and $Y(NO_3)_3$ solution with ethanol solvent, the mixing solution was stirred slowly with a drop of DEA solution and was sonificated. The investigation of the thermal conductivity and the densification nature of yttria coated AlN prepared by mechanical mixing and the above mentioned method was carried out and compared each other. Chemical mixing can be achieved in the following ways: (i) aqueous method, where the precipitation can be obtained from inorganic salts[38,39] or the hydrolysis of metal alkoxides by the addition of water,[40,41] (ii) by using proper polyelectrolyte or controlling the pH value, the hetero coagulation can be obtained between the oppositely charged particles.[42,43] Since, AlN powder is highly hydrolyzed in water, processing the AlN powder using the above mentioned methods is highly challenging.[44]

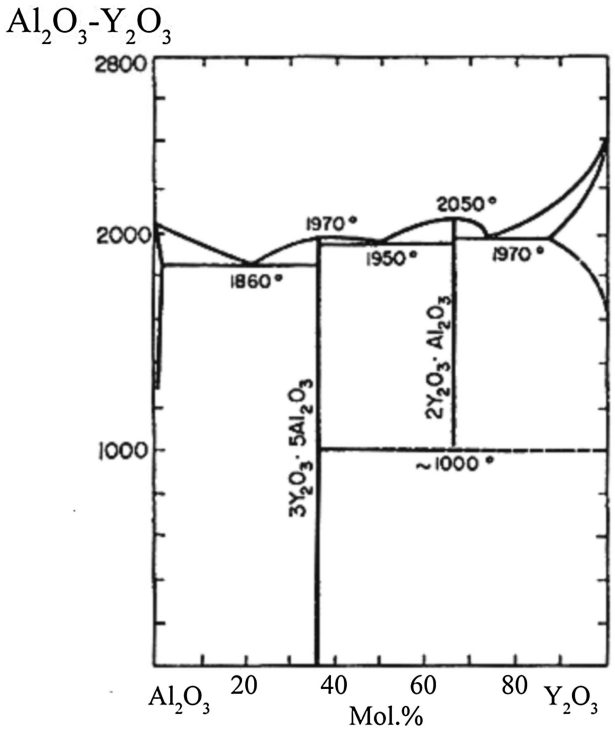

Fig. 1. Phase diagram explaining the formation of Y_2O_3–Al_2O_3 system.

DOI: 10.1002/adem.201400078

Table 2. Quantity of second phases of specimens with different morphologies. Reproduced with permission.[57] Copyright © 2005, John Wiley and Sons

Sintering condition	Amount of second phase [vol%]	Morphology of second phase
1900 °C, 2 h, fast cooling	4.84 (0.23)	Interconnected
1900 °C, 2 h, slow cooling	4.81 (0.26)	Isolated

Number in parentheses is standard deviation for 8–10 measurements.

2.3. Controlling Morphology of Second Phase

The thermal conductivity of AlN ceramic is highly affected by second phase morphology. The morphology of second phase of AlN can be controlled as an interconnected or isolated second phase with the cooling rate after sintering. In liquid phase sintered materials, the morphology of the second phase is determined by the ratio of the solid–solid interfacial energy to the solid–liquid one.[45] The isolated second phase morphology can be obtained by controlling the cooling rate after the sintering if the microstructural difference was due to the difference in the ratio of the interfacial energies with temperature. The thermal conductivity of the samples with different second phase microstructure was measured experimentally and compared with the theoretical thermal conductivity.

It is essential to add the additives to obtain high thermal conductivity of AlN ceramics. Thus, inclusion of additives leads to the formation of residual grain boundary phases, which greatly affects the thermal conductivity of AlN.[46,47] Clear identification of the morphology and its effect on the second phase to the thermal conductivity of AlN are highly challenging due to the purification of the AlN lattice may occur simultaneously with the microstructural change. By varying the additive content, sintering conditions, an oxygen content of AlN raw material, different microstructures of the grain boundary phases were obtained.[48–52]

It is known that the morphology of the grain-boundary phases is a function of the dihedral angle and volume fraction of the second phases.[53] The volume fraction of second phases for the specimens cooled at different cooling rates after sintering at 1900 °C is shown in Table 2. Table 2 indicates that the volume fractions of the second phases did not show large difference with cooling rates. The above observations clearly indicate that the morphological difference of the second phases between the slow-cooled and fast-cooled specimens was not triggered by the change of the composition or the volume fraction of the second phases.

Figure 2 shows the temperature profiles of Y_2O_3 doped specimens cooled at different rates after sintering at 1850 or 1900 °C in order to explore the morphological dependence of the second phases on the cooling rates. Fast-cooled specimens with the thermal history of Figure 2a had interconnected second phases, as shown in Figure 3a and b. Figure 3c and d shows the microstructures of the specimens heat treated through the thermal history of Figure 2b. This is clear evidence that the second phases were concentrated on the corners of the AlN grains and isolated from one another, if the cooling rate was slow.

Second phase forms as isolated pockets at the corners of the grain when the dihedral angle is >120. The second phase penetrates along the edges of three grains, when the dihedral angle is between 60 and 120. The relationship between the dihedral angle and temperature can be expressed as follows: $\cos(\psi/2) = 1/2(\gamma_{ss}/\gamma_{sl}), (\partial\gamma_{ss}/\partial T) = -S_{ss}, (\partial\gamma_{sl}/\partial T) = -S_{sl}$, where ψ is dihedral angle, γ_{ss} is the grain boundary energy, γ_{sl} is the solid–liquid interfacial energy, S_{ss} and S_{sl} are the entropies of the solid–solid and the solid–liquid interfacial energies, respectively. In general, the entropy of the solid is expected to be lower than that of solid–liquid interface.[54] Therefore, decreasing the temperature will lead to a decrease of the ratio $(\gamma_{ss}/\gamma_{sl})$ and hence an increase of the dihedral angle.[55] According to the above relationship, the formation of isolated second phases in the slow-cooled specimens is

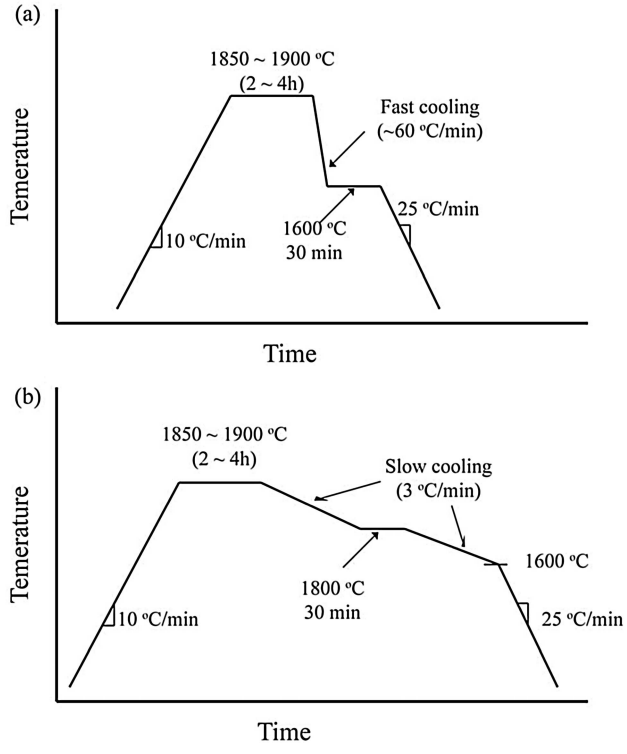

Fig. 2. Heating and cooling temperature profiles of a) the fast cooling and b) the slow cooling experiments. Reproduced with permission.[57] Copyright © 2005, John Wiley and Sons

DOI: 10.1002/adem.201400078

ADVANCED ENGINEERING MATERIALS

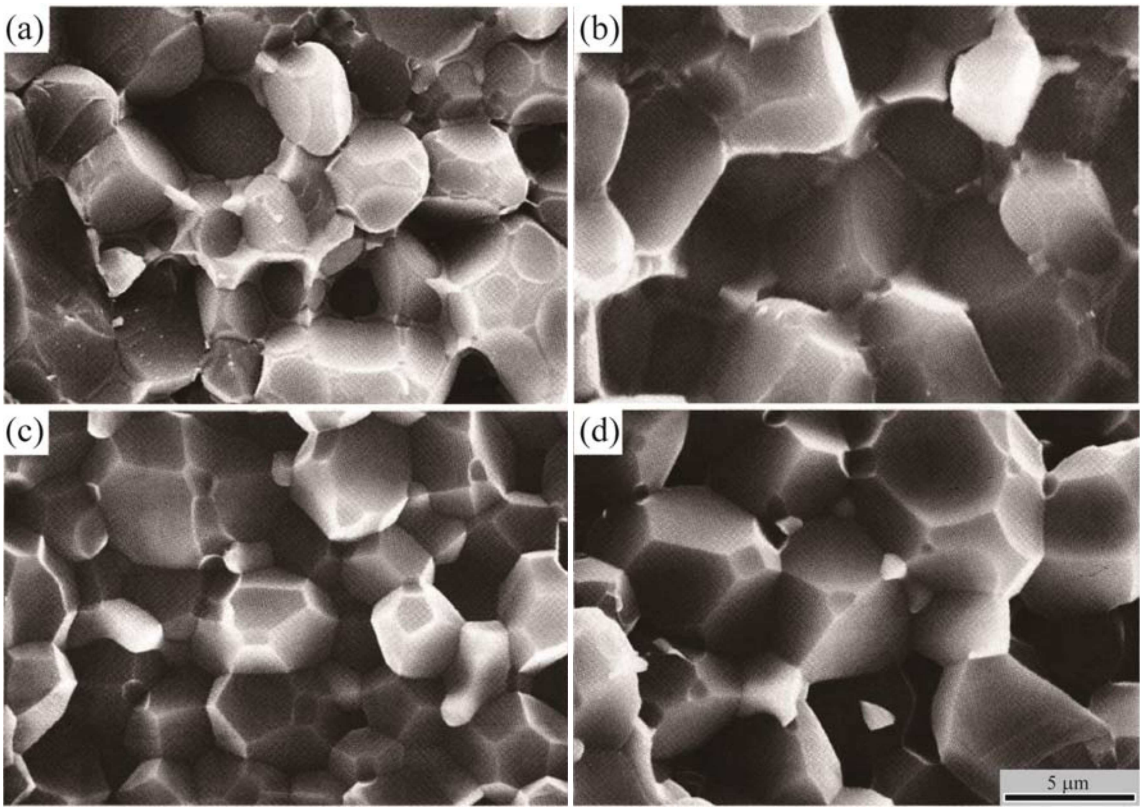

Fig. 3. SEM images of the AlN samples a,b) fast-cooled and c,d) slow-cooled after sintering at a,c) 1850 °C and b,d) 1900 °C for 2 h. Reproduced with permission.[57] Copyright © 2005, John Wiley and Sons

attributed to the decreases of $(\gamma_{ss}/\gamma_{sl})$ ratio during cooling. If the specimen is cooled at a fast rate, the changes in the morphology of the second phases might be kinetically limited due to the increase of the viscosity of the liquid phase. Therefore, a frozen-in second phase microstructure will be obtained. In order to confirm the above mentioned explanation, the slow and fast-cooled samples after sintering at 1900 °C for 2 h were reheated to 1900 °C with an isothermal holding period of 10 min and were cooled at an inverse rate. Figure 4a and b shows the microstructure of this sample. The interconnected second phase was withdrawn from the three-grain junctions and concentrated in the corners of the AlN grains. In contrast, Figure 3d shows the isolated structure of the second phase changed into the interconnected structure (Figure 4b) by fast cooling after reheating to 1900 °C. From all the observations, we can conclude that the second phase's morphological changes were caused mainly by the modification of the ratio of the solid–solid interfacial energy to the solid–liquid one during cooling.

The thermal conductivity of AlN samples was calculated from modeled microstructures that have isolated and interconnected second phases. The model proposed by Buhr and Müller[50] was employed for the microstructure of the interconnected second phase. According to this model, the grains (AlN) are assumed to be part of a periodic stacking of cubes with beveled edges and second phases in the channels along the grain edges, forming prisms. On the other hand, the Maxwell model was employed to calculate the thermal conductivity of the microstructure with isolated pockets of second phases.[56]

In order to compare the experimentally measured thermal conductivity to the calculated one from above mentioned models, the amount ($V_{SE,}$ volume fraction) of second phase and the thermal conductivity of AlN grain (K_{AlN}) have to be known. V_{SE} and K_{AlN} values were obtained by employing the micrographs of the polished surfaces using an image analyzer, and from the contents of the lattice oxygen, which were measured by the selective hot-gas extraction method through the following equation: $K_{AlN}^{-1} = K_{AlN,theor}^{-1} + C.(\Delta n/n_0)$, where $K_{AlN,theor}$ is the theoretical thermal conductivity (=319 W m^{-1} K^{-1}) of a pure AlN single crystal, C a constant (0.43), Δn the number density of the oxygen impurities (atoms cm^{-3}), and n_0 the number density of the nitrogen atoms in AlN ($=4.79 \times 10^{22}$ atoms cm^{-3}). Selective hot-gas extraction analysis was carried out for the fast-cooled samples after sintering at 1850 °C for 4 h and for those slow-cooled samples after sintering at 1850 °C for 2 h. The obtained results are shown in Table 3. It is obvious that the amount of lattice oxygen decreases when the yttria content and the sintering time increases. This observed result agrees well with the results shown by Virkar *et al.*[30] According to Virkar *et al.*, purification of the AlN lattice is favored by the reduced

REVIEW

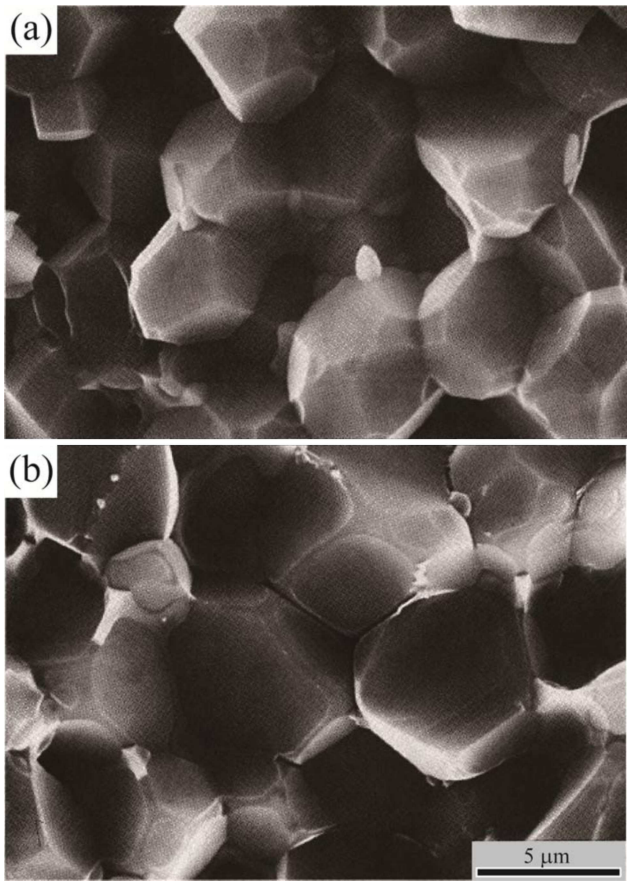

Fig. 4. Samples of Fig. 3b and d were heat treated, at 1900 °C. a) Slow-cooled and b) fast-cooled specimens. Reproduced with permission.[57] Copyright © 2005, John Wiley and Sons

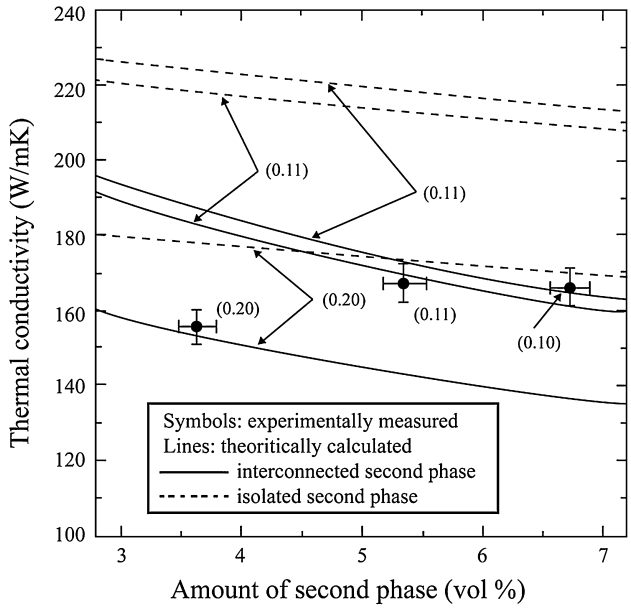

Fig. 5. Calculated (Buhr and Muller model) and measured thermal conductivity values as a function of the amount of the second phase for the fast-cooled specimens after the sintering was carried out at 1850 °C for 4 h. The measured thermal conductivities are well matched with the calculated values. The numbers in parentheses represent the oxygen content in the AlN lattice. Reproduced with permission.[57] Copyright © 2005, John Wiley and Sons

Al_2O_3 activity in the second phase and is also related to kinetic factors.

Another important feature that can be seen in Table 3 is that the slow-cooled AlN specimens exhibit higher thermal conductivity than the fast-cooled ones, regardless of the higher content of the lattice oxygen.[57] The observed results clearly indicate that the thermal conductivity of AlN is greatly affected by the morphology of the second phase. Figure 5 and 6 show the calculated thermal conductivity from the content of the lattice oxygen, which is plotted as a function of the volume fraction of the second phase. Figure 5 and 6 show the thermal conductivity plots of specimens with interconnected and isolated second phases respectively. The thermal conductivity values obtained from the calculation employing the Buhr and Muller model agree well with the measured thermal conductivity values of interconnected phases (Figure 5). On the other hand, Figure 6 shows the measured thermal conductivity values of the samples with isolated second phase microstructure, which are close to the dashed lines. From all the above observations, we can clearly see that the thermal conductivity of AlN ceramics can be improved by changing the morphology of the second phase into an isolated structure, even if AlN ceramics have a large amount of second phase.

Table 3. Quantity of second phases, oxygen contents in the AlN lattice. Reproduced with permission.[57] Copyright © 2005, John Wiley and Sons

Sintering condition	Content of Y_2O_3 [wt%]	Amount of second phase [vol%]	Content of oxygen [wt%]	Thermal conductivity [$W\,m^{-1}\,K^{-1}$]
1850 °C, 4 h, fast cooling	2	3.64 (0.32)	0.20 (0.03)	155.8 (4.7)
	4	5.35(0.36)	0.11 (0.03)	165.5 (5.0)
	5	6.72 (0.32)	0.10 (0.02)	166.4 (5.0)
1850 °C, 2 h, slow cooling	2	3.34 (0.40)	0.25 (0.03)	159.1 (2.4)
	4	5.27 (0.33)	0.19 (0.03)	173.1 (2.6)
	5	6.47 (0.38)	0.19 (0.03)	174.9 (2.7)

Thermal conductivity of AlN samples with different morphologies of second phase is also shown.
Number in parentheses is standard deviation.

DOI: 10.1002/adem.201400078

ADVANCED ENGINEERING MATERIALS

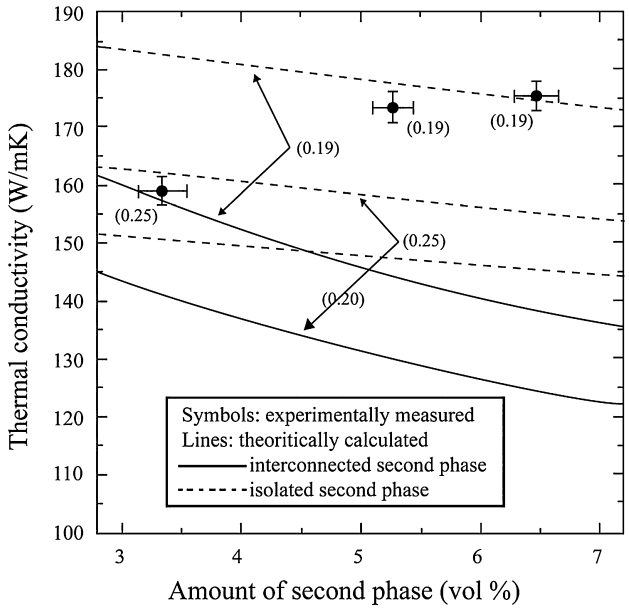

Fig. 6. Calculated and measured thermal conductivity values as a function of the amount of the second phase for the fast-cooled specimens after the sintering was carried out at 1850 °C for 2 h. The measured thermal conductivities are well matched with the calculated values (Maxwell model). The numbers in parentheses represent the oxygen content in the AlN lattice. Reproduced with permission.[57] Copyright © 2005, John Wiley and Sons

2.4. Minimizing the Second Phase

The thermal conductivity of AlN ceramics is affected by the following factors: (i) defects related to oxygen in the lattice, (ii) the amount of lattice oxygen present, and (iii) the low thermal conductive second phases segregated in grain boundary. It has been reported (Fujimoto and Ueda) that adding $CaCO_3$ into AlN ceramics that were heat treated at 1100 °C for 5 h (CF_4 gas atmosphere) after the sintering at 1900 °C for 6 h in N_2 atmosphere exhibits the thermal conductivity of 230 $W\,m^{-1}\,K^{-1}$ because the second phases located in grain boundary are driven off.[46] Enloe *et al*. have employed auger electron spectroscopy (AES) to analyze the thickness (2–100 nm) of the second phase present in the grain boundaries and the effect of sintering conditions and the type of additives on the thermal conductivity of AlN ceramics. They have concluded that the thermal conductivity decreases with increasing the thickness of the film.[45] Nakano *et al*.[58] reported a thermal conductivity value of 272 $W\,m^{-1}\,K^{-1}$ by adding Y_2O_3 into AlN, which can be obtained by reducing the amount of grain boundary phases through heat treatment at 1900 °C for 100 h. It is clear from the above studies that prolonged heat treatment and employing a reducing atmosphere are very essential to improve the thermal conductivity of AlN. However, prolonged annealing time and reducing atmosphere increase the amount of second phase segregated in the grain boundary phase which cause reduction of thermal conductivity. Through prolonged heat treatment and reducing sintering atmosphere, the amount of second phase can retain or enhance the thermal conductivity.

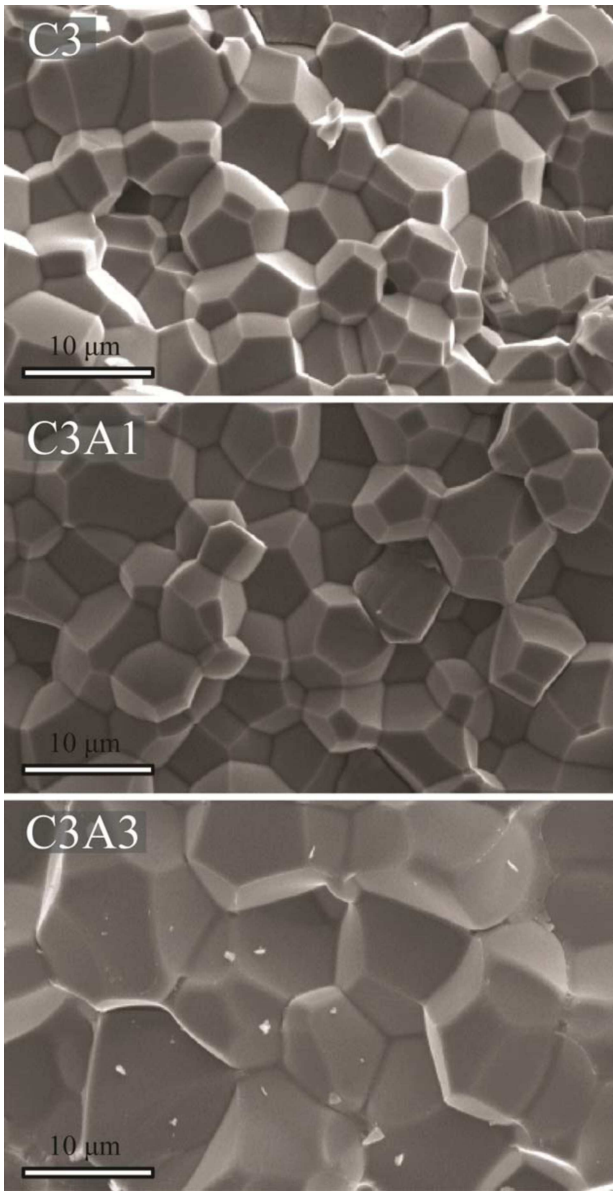

Fig. 7. SEM micrograph images of a fracture surface in specimens C3, C3A1, and C3A3. The second phases was not seen to form at the grain boundaries in all specimens. Reproduced with permission.[29] Copyright © 2005, John Wiley and Sons

Calcium fluoride (CaF_2) is another promising sintering additive that can increase the densification of AlN at low temperature sintering and enhance the thermal conductivity by minimizing the second phase. With the inclusion of CaF_2, the formation of second phase can be suppressed and the thermal conductivity of AlN can be enhanced. Figure 7 shows the SEM micrographs of three sintered AlN ceramics (specimens C3, C3A1, and C3A3). There were no second phases at the grain boundaries of AlN ceramics found with the inclusion of CaF_2 additives. The reason for not observing any second phase could be as follows: CaF_2 is volatile above 1600 °C and the liquids phases composed of CaF_2 might have evaporated during high temperature sintering. CaF_2 is

DOI: 10.1002/adem.201400078

expected to react with AlN and form a gas phase of Ca and AlF_3 as follows:

$$3CaF_2\,(s) + 2AlN\,(s) = 3Ca\,(g) + 2AlF_3\,(g) + N_2\,(g) \quad (1)$$

At 1600 °C, the vapor pressure of Ca (g) is sufficiently high (0.1 mbar) and the sublimation of AlF_3 begins at around 1250 °C[59] resulting in the formation of pure phase without any second phase after the sintering at 1900 °C. CaF_2 reacts with other sintering additives and does not remain in the second phase in grain boundaries because it effortlessly evaporates above 1650 °C. Liu *et al.*[60] have reported that the thermal conductivity of AlN ceramics increases as contents of CaF_2 increase up to 2 wt% simultaneously using YF_3 and CaF_2 additives. Microstructural analysis reveals that CaF_2 evaporates above the sintering temperature of 1650 °C. In addition, they have shown that the $(Ca,Y)F_2$ phase forms and becomes liquid above 1400 °C in the CaF_2–YF_3 system and then the liquid phase makes YF_3 react with oxygen more effectively. At high temperatures and under a nitrogen atmosphere, CaF_2 is expected to evaporate due to its high vapor pressure at 1600 °C (about 1 mbar). In order to overcome this problem, we have included assistant sintering additives (Al_2O_3) that can control the volatilization of CaF_2, and we used BN plates instead of BN bed powder.

Figure 8 shows the density and the thermal conductivity (as a function of CaF_2) of AlN ceramics sintered at 1900 °C for 3 h in the atmosphere changed by using BN plates. Thermal conductivity is seen to increase rapidly with increasing CaF_2 contents and when the added CaF_2 contents is 2 wt%, the thermal conductivity shows the highest thermal conductivity value of 211 W m^{-1} K^{-1}. When the amount of CaF_2 exceeds 2 wt%, the thermal conductivity decreases. The density of the AlN specimen with the inclusion of very small CaF_2 contents (0.1 wt%) is seen to have the value of 3.216 g cm^{-3}, which is the nearly theoretical density of AlN ceramics. At the same time, the density of the AlN specimen without any CaF_2 addition is seen to have the value of 2.732 g cm^{-3}. Increasing CaF_2 to a value of 1.5 wt%, the density of the AlN specimen increases. However, the density of the AlN specimen decreases with increasing CaF_2 content above 3 wt%. By increasing CaF_2 content, the driving force of CaF_2 evaporation increases and it evaporates with AlN, leading to the decrease of the density of AlN samples. The thermal conductivity is seen to depend highly on the density of AlN samples. When the CaF_2 amount goes above 3 wt%, the density of the AlN specimen decreases and the thermal diffusivity also decreases by evaporation of CaF_2. Figure 9 shows the density and thermal conductivity of the 3 wt% of CaF_2 added specimens as a function of Al_2O_3 contents. High thermal conductivity (190.4 W m^{-1} K^{-1}) and high density values (>95%) of AlN ceramics were obtained with 3 wt% CaF_2 additives. Inclusion of Al_2O_3 leads to an increase in the density of AlN to 3.23 g cm^{-3}. Inclusion of a small amount of Al_2O_3 into AlN increases the thermal conductivity by facilitating liquid phase sintering. However, by increasing the amount of Al_2O_3 above certain value,

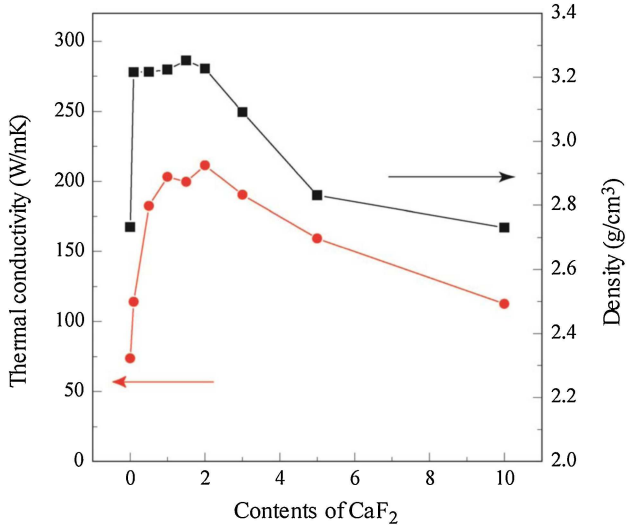

Fig. 8. The thermal conductivity and density values of 3 wt% CaF_2 doped AlN ceramics with 0, 1, and 3 wt% added Al_2O_3.

thermal conductivity decreases due to the increase in oxygen related defects by the solid solution of Al_2O_3 into AlN grain. Figure 9 shows that C3 (CaF_2–3 wt%) specimen yielded a higher thermal conductivity of 190.4 W m^{-1} K^{-1}, and the C3A3 (CaF_2–3 wt% + Al_2O_3–3 wt%) specimen yielded a value of 173.3 W m^{-1} K^{-1}.

3. Characterization

3.1. Measurement of Thermal Conductivity

The laser flash method is generally used for measuring the high-thermal conductive material. Thermal diffusivity of materials is measured by the laser flash method. An energy pulse heats one side of a parallel sample. The light source heats the sample from the bottom side and a detector on top

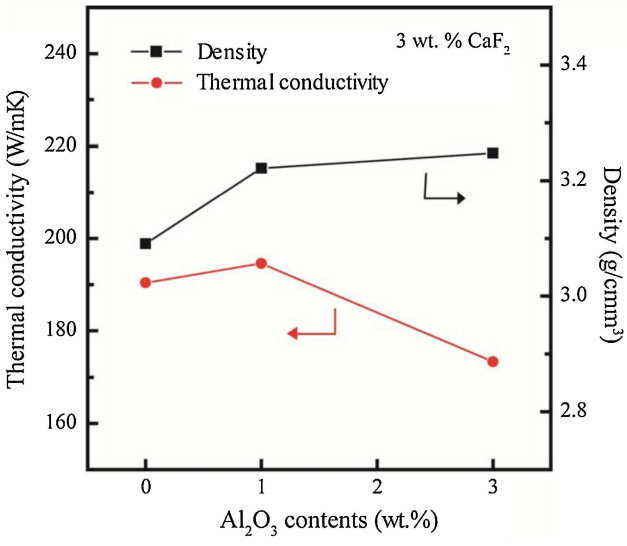

Fig. 9. The measured density and the thermal conductivity values (as a function of CaF_2 amount) of AlN ceramics sintered at 1900 °C for 3 h. Reproduced with permission.[29] Copyright © 2005, John Wiley and Sons

DOI: 10.1002/adem.201400078

detects the time-dependent temperature rise. The higher the thermal diffusivity of the sample, the faster the energy reaches the backside. A laser flash method containing a glass-Nd laser and an InSb infrared sensor was employed to measure the thermal diffusivity of all the samples at room temperature.[61] The accuracy of the apparatus is ±3%. Typical sample dimensions were 12 mm in diameter and 2–3 mm in thickness, and both sides of the specimens were sputter-coated with gold to a thickness of 0.1 μm. A thin layer of colloidal carbon was spray-deposited onto the gold layers to enhance the absorption of the laser pulse and the emissivity of the rear surface of the specimen. The thermal conductivity was calculated from the equation $K = C.\rho.d$, where C is the heat capacity (718 J $kg^{-1} K^{-1}$), ρ is the density, and d is the thermal diffusivity of the specimen. The reported thermal conductivity is an average of three measurements.

A structural analysis was carried out employing X-ray diffractometry (XRD) with Cu Kα radiation. The dihedral angle at the intersection of the second phase and the grain boundary was measured on several TEM micrographs. Several repeated measurements (about 50 measurements) were carried out to determine the dihedral angle TEM scanning electron microscopy (SEM) was employed to analyze the microstructures on the fracture surfaces of the sintered pellets using. Employing an image analyzer attached to the SEM, the volume fraction of the second phases was determined on the polished surfaces.

3.2. Lattice thermal conductivity from Raman spectra

The defects present in AlN samples (single-crystal and polycrystalline form) are the oxygen-related defects consisting of oxygen substitution for nitrogen (O_N), aluminum vacancies (V_{Al}), and $O_N - V_{Al}$ complexes. The thermal conductivity of AlN can be largely influenced by the accommodation of oxygen in the lattice. However, there is no clear report on the role of oxygen and oxygen-related-defects on the thermal conductivity of AlN. The diffusion of phonons through the solid is the main reason for the thermal conductivity in insulators and semiconductors. Therefore, the thermal properties of the solid mainly depend on the phonons, which are largely affected by the nature and amount of native defects and impurities in the material. The poor treatment of anharmonic effects in AlN samples, which occur together with the defect affects the controlling phonon lifetime.[62,63]

Raman spectroscopy is a very valuable tool to study the phonon interactions and their dynamics, as well as the factors influencing them. In the Raman spectra, line width is associated with the phonon mean free path.[64,65] Recently, Bergman *et al.*[66] reported that by incorporating Si and C impurities into AlN matrix, micro-Raman line widths become about 50% broader. McCullen *et al.*[67] have reported that the broadening of E_2 (high) and E_2 (low) Raman lines is associated with oxygen concentrations in the AlN films. From these studies, it is clear that the presence of defects and impurities in AlN causes the broadening of Raman line width due to the combined effects of anharmonic decay, which determines the intrinsic line width, and point defect scattering. The measured full width at half maximum (FWHM) can be associated with the scattering associated with point defects if there are no strong stress gradients in the material during the measurement. In our group, a detailed FT-Raman spectroscopy study was carried out on yttria-doped polycrystalline AlN ceramics. The line broadening of Raman line width and the thermal conductivity of AlN grains calculated from the bulk thermal conductivity of AlN was compared. In addition, the width of Raman lines of the E_2 (high) phonon were related to the oxygen-related defects and impurities, as measured from the lattice parameter through XRD.

Figure 10 shows the FT-Raman spectrum of three samples NY1, 3, 5 having different Y_2O_3 content (nano-Y_2O_3 doped 1, 3, and 5 wt%). Raman spectra were measured in the energy range of 200–1000 cm^{-1}. The peaks detected at around 612, 658, and 666 cm^{-1} can be assigned to the A_1 (TO), E_2 (high), and E_1 (TO) modes, respectively for all the AlN samples.[68] Raman active modes corresponding to the vibrations of the Al sublattice and N atoms cause nonpolar E_2 (low) and E_2 (high) modes in the spectrum.[69–71] The strongest mode among all the modes is seen to be E_2 (high) mode in the polycrystalline AlN wurtzite structure and it was used to relate the peak broadening to defects or impurities. A Lorentzian fit was carried out on the E_2 (high) mode peaks to calculate the Raman line width (FWHM), because the line shape of the phonon mode can be approximated by a Lorentzian fit. The line widths of the E_2 (high) mode ranged from 6.5 to 7.9 for all the AlN pellets. These values were found to be greater

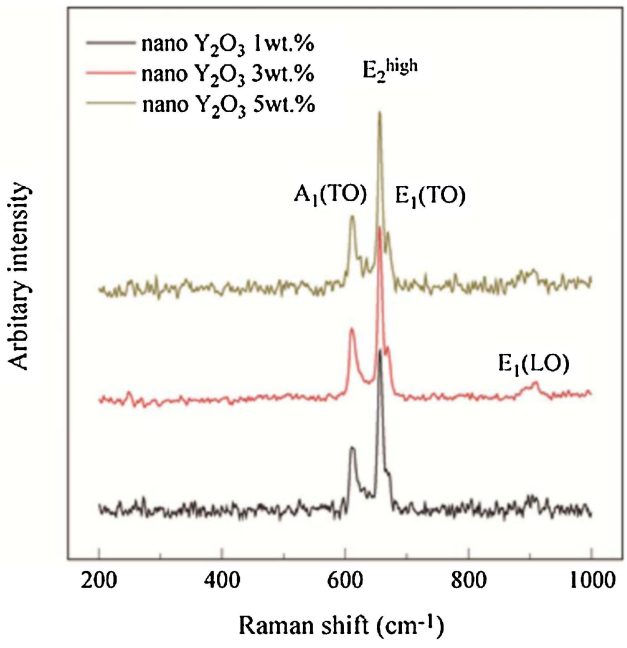

Fig. 10. Room temperature Raman spectrum of nano Y_2O_3-doped AlN sintered at 1900 °C for 3 h. Reproduced with permission.[28] Copyright © 2005, John Wiley and Sons

DOI: 10.1002/adem.201400078

REVIEW

than the line width value of 3 cm^{-1} for an AlN single crystal of high perfection.[44] The above observation clearly showed that the polycrystalline AlN ceramics used in the present study contained a considerable amount of phonon scattering sources, which can be related to the oxygen defects or some impurities, compared with single crystalline AlN. In polycrystalline AlN ceramics, defects related to oxygen and impurities occur in the AlN grains. Oxygen-related defects are mainly formed by the substitution of oxygen atoms for N atoms. This oxygen substitution affects the local crystalline electric field due to alloy electric potential variations resulting from the loss of the translational constant, leading to the collapse of the wave vector (the $q = 0$ Raman selection rule). Therefore, the broadening of Raman peaks observed in the present case is a result of the light scattering from the entire Brillouin zone. The phonons scattered by Si impurity, which is placed at the Al ion, would be negligible. However, every three Si ions there should be a cation vacancy, and this defect could be a phonon scattering source.[72] Therefore, the Raman line width is affected when an impurity arises at the Al ion site or oxygen occupies an N site. The properties of AlN ceramics doped with Y_2O_3 are shown in Table 4.

The formation of Al vacancies leads to lattice contraction, which was confirmed by measuring the *c*-axis lattice constant value. The relationship between the Raman line width and the defects present in AlN samples was correlated via the changes in the lattice parameter values. The presence of defects and impurities in AlN samples leads to the formation of vacancies (aluminum vacancies) to maintain the charge neutrality. From X-ray data by using the Cohen least squares method, one can analyze the relationship between the Raman line width and the defects.[73]

The X-ray diffraction peaks (205) of the three selected samples are shown in the inset of Figure 11, which had Raman line widths of 6.5, 7.3, and 7.9 cm^{-1}, respectively. Figure 11 shows a variation of the lattice parameter with the line width of the E_2 (high) mode. The (205) peak is seen to shift towards the lower angle side for the samples with larger Raman line width of E_2 (high) modes, which confirmed that an increasing number of Al vacancies were formed by point defects and impurities. From the above observation (Figure 11) a correlation between the Raman line width and the changes in *c*-axis lattice parameter caused by the amount of aluminum vacancies is obtained.

Figure 12 shows the correlation between the line width of the E_2 (high) Raman mode and the lattice thermal conductivity. In general, the following factors affect the thermal conductivity of polycrystalline AlN ceramics: defects in the grain, sintering additives, and the presence of a second phase. Defects, such as impurities within the AlN grain or oxygen-related defects, affect the lattice thermal conductivity. Buhr and Muller's interconnected second-phase model was employed to calculate the lattice thermal conductivity from the bulk thermal conductivity of the AlN samples used in this study. By increasing the sintering additives, thermal conductivity increases. The AlN grains used in the present study are around 5–10 μm, and the phonon mean free paths were too small compared to the variation in grain size; therefore, the effect of grain size on the lattice thermal conductivity is negligible. The lattice thermal conductivity was considered to investigate the effect of point defect scattering on the thermal conductivity of AlN grains. A linear relationship between the E_2 (high) mode line and the lattice thermal conductivity was obtained in the present study. Taking the the theoretical thermal conductivity (319 $W\,m^{-1}\,K^{-1}$) of AlN into account, the linear fitting equation of the data can be represented as $K = 319 - \alpha(\tau - \beta)$, where τ is the Raman line width.[28] The variables α and β are determined from a linear regression fit of the lattice thermal conductivity results, and their values are $\alpha = 94\ W\,m^{-1}\,K^{-1}$ $\beta = 5.6\ cm^{-1}$. β is the Raman line width (FWHM) of the mode, which is the intrinsic line width caused

Table 4. Microstructure, thermal conductivity and Raman line width of AlN Samples prepared by using nano- and micro-sized Y_2O_3 and yttrium coating.

	Grain size [μm]	Vol%	Thermal conductivity [$W\,m^{-1}\,K^{-1}$]	Raman linewidth [cm^{-1}]
MY1	5.81	0.7	94.5	7.86
MY3	5.07	1.7	167	7.12
MY5	6.32	3.1	131.5	7.33
NY1	5.90	0.5	110.7	7.74
NY3	5.81	1.5	177.8	6.81
NY5	6.43	3.3	185.1	6.50
NY1–2	6.21	1.1	110.2	7.59
NY3–2	4.39	1.5	191.7	6.42
CY1	4.56	1.9	178.2	6.74

All the samples were sintered at 1900 °C for 3 h.

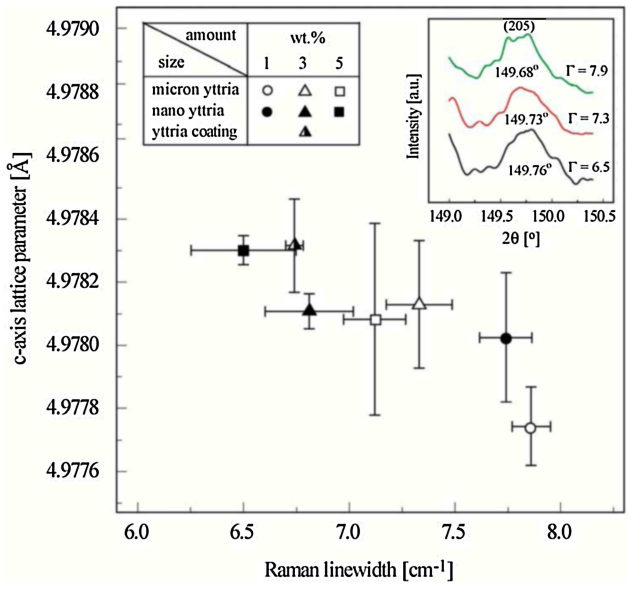

Fig. 11. Relationship between the Raman line width of the E_2 (high) mode and c-axis lattice parameter value. The inset shows the (205) XRD peaks of three selected samples. Reproduced with permission.[28] Copyright © 2005, John Wiley and Sons

DOI: 10.1002/adem.201400078

ADVANCED ENGINEERING MATERIALS

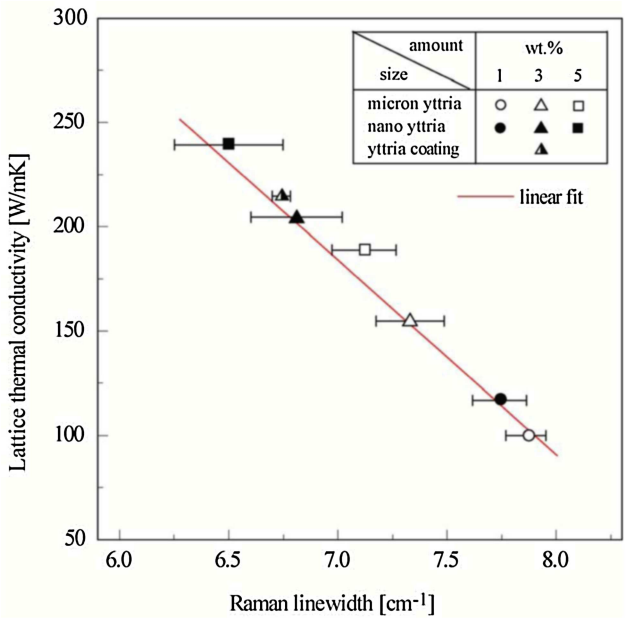

Fig. 12. Relationship between the Raman line width of the E_2 (high) mode and the lattice thermal conductivity for the different amount of additives and sizes of yttria doped AlN ceramics. Reproduced with permission.[28] Copyright © 2005, John Wiley and Sons

by the effect of the anharmonin decay of AlN. The intrinsic line width (β) values calculated from the above relationship are larger than the value of 3 cm^{-1} for highly perfect single crystalline AlN (measured by micro-Raman spectroscopy). The broadening of the intrinsic Raman line width of polycrystalline AlN could be due to the scattering sources such as the second phase between AlN grains or grain boundaries because of the larger laser spot size and depth of focus used in the FT-Raman spectrometer. In addition to that, a detailed investigation on the intrinsic line width of polycrystalline materials is being carried out.[28] The effect of point defect scattering in polycrystalline AlN ceramics was incorporated in Equation 8 by subtracting the β-value from the Raman line width obtained.

3.3. Electrical Conductivity by High Temperature AC Impedance Spectroscopy

For all the impedance measurements, thin silver film was deposited and dried on both sides of the specimen, which served as electrodes. The silver film was deposited on a circular area (1.0 mm diameter) at the center of the pellet. The silver electrode-coated specimen was sandwiched between platinum foils, which were connected to platinum wires in a spring-loaded specimen holder. The electrical properties were measured by impedance spectroscopy at amplitude of 1000 mV (Solartron 1260, Farnborough, UK) over a decreasing frequency range from 13 MHz to 5 Hz, and over the temperature range of 200 to 500 °C for CaF_2-doped AlN ceramics. For every 25 °C interval, impedance spectra were collected and analyzed. In order to achieve thermal equilibrium at every measurement, temperature was maintained for a sufficient time (20 min) before the data was collected. The total impedance was resolved into real (Z') and imaginary (Z'') parts, and Cole–Cole plots were constructed to analyze the data.

Several studies on the thermal conductivity and the factors affecting the thermal conductivity of AlN have been carried out over the past few decades.[74,75] However, the electrical conductivity and the electrical conduction mechanism of AlN ceramics have not been thoroughly studied and not yet understood completely. In our group, the electrical properties of AlN ceramics doped with CaF_2–Al_2O_3 additives were investigated by high-temperature AC impedance spectroscopy, considering the existence of a grain-boundary amorphous phase. Controlling and manipulating the electrical resistivity of AlN ceramics becomes important when these ceramics are used for electrical and electronic device applications. When the thermal conductivity of AlN is kept high, the electrical resistivity must be maintained within the desired range. Kusunose *et al.*[74] showed that, by precipitating a yttrium oxycarbide grain boundary phase, it is possible to solidify electrically conductive AlN ceramics without losing their intrinsic high thermal conductivity. Yoshikawa *et al.*[75] reported the room temperature electrical resistivity of Sm_2O_3 doped AlN ceramics employing a DC three-pole method. They have demonstrated that the three-dimensional network of the grain boundary phase of Sm-β-alumina controls the electrical conductivity of AlN ceramics and the order of resistivity is 10^{10}–10^{14} Ω cm. The above mentioned reports showed that the electrical conductivity of AlN ceramics and their variation is determined by both the structural and electrical properties of the second phase at grain boundaries; however, a detailed investigation of the electrical conductivity of AlN ceramics is missing.

A simplified brick layer model was employed to analyze the electrical properties of the polycrystalline AlN ceramics. According to the model, polycrystalline solid is represented by cubic grains, which are separated by flat grain boundaries. The polycrystalline sample can be represented using an equivalent circuit and the number of resistor–capacitor (RC) elements in the equivalent circuit represents the number of different microstructural components in the material, such as AlN grains, grain boundaries, pores, electrodes, and precipitates. If there are no precipitates or electrode polarization effects on the impedance, only the RC branches representing grains and grain boundaries exist in the equivalent circuit. Based on the following equation, the net grain boundary resistivity (ρ_{gb}) and grain resistivity (ρ_{grain}) values were calculated: $\rho_{grain} = R_{grain}\ A/t$, $\rho_{gb} = R_{gb}\ A/t$, where A is the effective electrode area and t is the specimen thickness.

The specific grain boundary resistivity (average resistivity of a single grain, ρ_{gb}^{sp}) can be related to the grain size (d_g), the net grain boundary resistivity (ρ_{gb}), and the thickness of the grain boundary (δ_{gb}) by the following equation: $\rho_{gb}^{sp} = \sigma_{gb}\ d_g/\delta_{gb}$.

Complex impedance spectra of the C3 and C3A3 samples (at 350 °C) are shown in Figure 13. The contributions from the

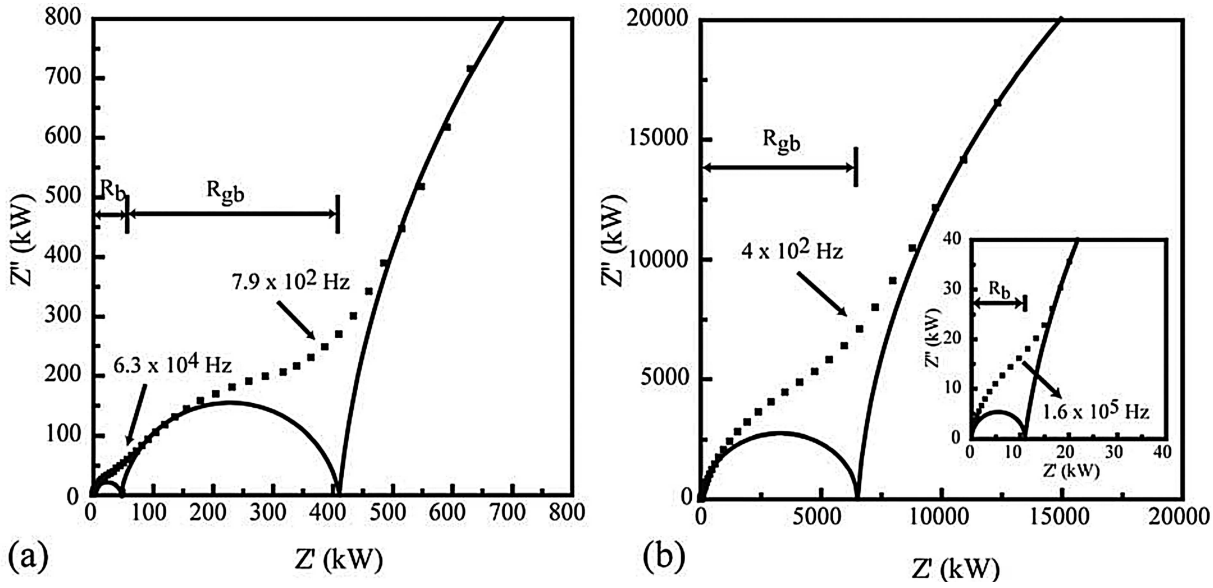

Fig. 13. AC impedance spectrum of the samples a) C3 and b) C3A3 at 350 °C. Reproduced with permission.[29] Copyright © 2005, John Wiley and Sons

grain, the grain boundary and the electrode to the observed impedance (three semicircles) are clearly indicated in the figure. The grain boundary resistivity of the C3 specimen is seen to be slightly higher than the resistivity of the grains. In the case of C3A3, the grain boundary resistivity is seen to be much higher than the grain resistivity (Figure 13b). These observations clearly show that the addition of Al_2O_3 has an effect on grain boundary resistivity. Resistivity corresponding to grain and grain boundaries are shown in Figure 14a, and a comparison is made. The resistivity corresponding to the grain boundary is seen to be four orders of magnitude higher than the grain resistivity. By increasing the Al_2O_3 amount, the resistivity of the grain boundary is seen to increase. In addition to that, the variation in grain resistivity is observed to be much smaller than that of the grain boundary. Figure 14b shows the ratio between the grain boundary resistivity and the grain resistivity of the C3, C3A1, and C3A3 samples. The grain boundary blocking effect on electrical conduction can be obtained from the above relationship. It is clear from Figure 14a that the sample C3A1 exhibits one order higher grain boundary resistivity than that of the C3 specimen, but the ratio between the grain boundary resistivity and the grain

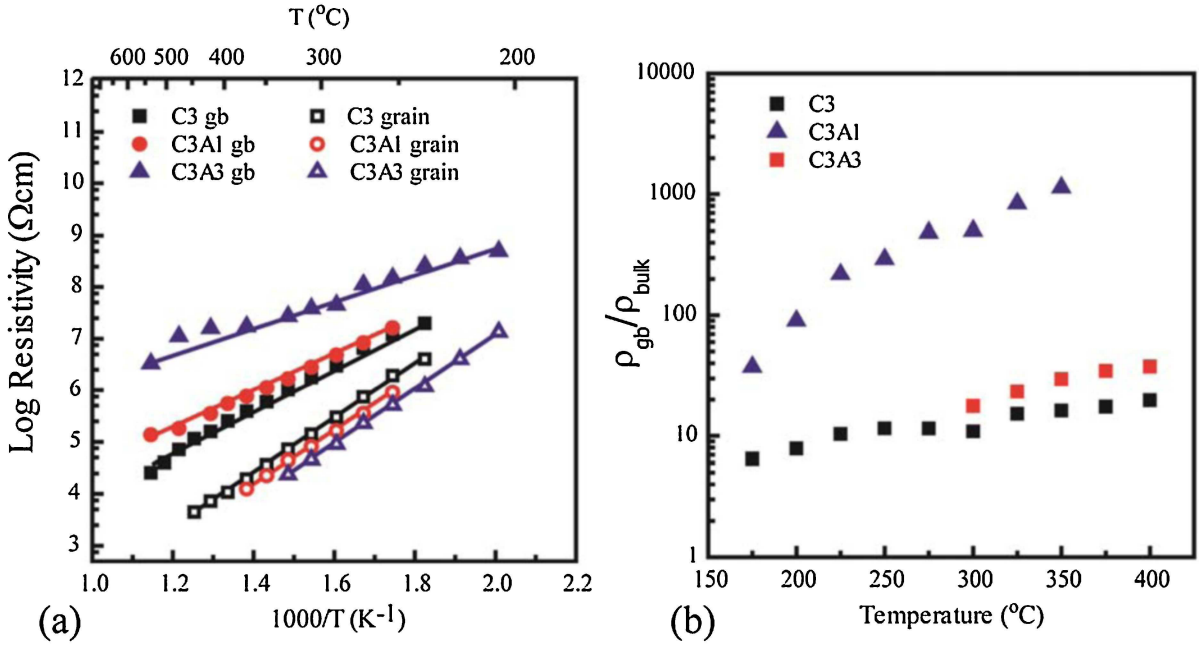

Fig. 14. a) Grain and grain boundary resistivity values as a function of temperature for CaF_2-doped AlN ceramics with added Al_2O_3, and b) the ratio between the grain boundary resistivity to the grain resistivity. Reproduced with permission.[29] Copyright © 2005, John Wiley and Sons

DOI: 10.1002/adem.201400078

resistivity is only a little higher than that of the C3 specimen. These observations show that that the high electrical resistivity of the C3A1 specimen was produced by high grain resistivity, not the grain boundary or the blocking effect due to the addition of a small amount of Al_2O_3. However, the large amount of Al_2O_3 containing the C3A3 specimen exhibits 50–1000 times higher grain boundary resistivity than that of grain resistivity. In the measured temperature range, the ratio between the grain boundary resistivity to the grain resistivity for the C3A3 specimen is higher than that of the C3 specimen. This observation showed that the grain boundary blocking effect on the electrical conduction was higher for the C3A3 specimen. In the CaF_2-doped (with 3 wt% Al_2O_3) AlN sample, electrical resistivity is seen to increase up to three orders of magnitude but the thermal conductivity decreases slightly owing to the formation of solid solution of Al_2O_3 within the AlN grain (by $< 10\%$).

TEM analysis of the C3 and C3A3 samples (added with Al_2O_3) was carried out to analyze the source of the grain boundary blocking effect. Figure 15 shows the TEM images of C3 and Al_2O_3 added C3A3 samples. The grain boundaries of C3 samples are quite clean (Figure 15a). High-resolution TEM (HRTEM) revealed that the well-crystallized grain boundaries have no traces of the segregation of atoms or amorphous/glassy phases in the grain boundaries. The C3 specimen with free grain boundaries (without any second phase) exhibits direct grain-to-grain contact. Except aluminum and nitrogen elements, calcium atoms were not observed within the grains.

An amorphous phase is seen to occur along the grain boundaries for the C3A3 sample and is shown in Figure 15c. The second phase is seen to have Al, O, and small amounts of Ca (0.53 wt%) in it. HRTEM analysis revealed that the C3A3 sample exhibits no other phase between the amorphous phase and the AlN grain. It is known that, with the inclusion of additives (Al_2O_3), amorphous phase might form along grain boundaries.[76,77] The activation energies corresponding to the grain and the grain boundary resistivity were calculated to conclude the effect of the amorphous phase at the grain boundary on the total electrical resistivity. The activation energies corresponding to the grains of the samples C3, C3A1, and C3A3 are found to be 0.95, 1.06, and 1.09 eV, respectively. The concentration of charge carriers for electrical conduction in the C3A1 and C3A3 specimens changed compared with the concentration of the charge carriers in the C3 specimen by

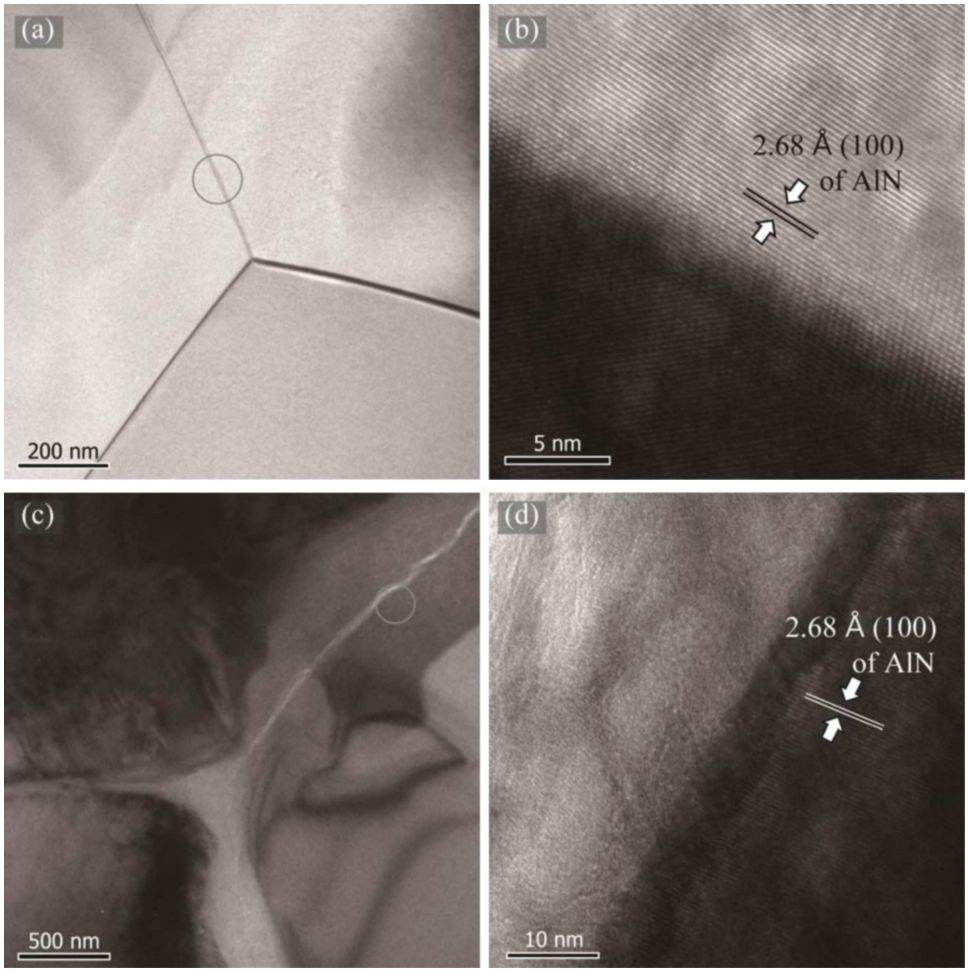

Fig. 15. TEM micrograph images of specimens a) C3 and b) C3A3 and HRTEM image of c) C3 and d) C3A3. In the C3A3 specimen, an amorphous phase is seen to occur along the grain boundaries. Reproduced with permission.[29] Copyright © 2005, John Wiley and Sons

transformation of Al_2O_3 solid solution into AlN grains during the sintering process. The activation energies corresponding to the grain boundaries of C3, C3A1, and C3A3 were calculated to be 0.67, 0.44, and 0.37 eV, respectively. Grain boundary activation energies were found to be lower than those of grains and they reveal that the CaF_2-doped AlN samples have a high electrical resistivity at high temperatures. Al_2O_3 added samples were found to have insulating amorphous phase at the grain boundaries without grain-to-grain contact, resulting in high grain boundary resistivity and low activation energy. The grain boundary activation energy is seen to be diverse for different samples, which indicate that the grain boundary blocking mechanism for electrical conduction is different in each case. From the microstructural analysis, Al_2O_3-added C3A3 sample exhibits the grain boundary blocking effect because of the presence of the amorphous phase at the grain boundaries.

In the equivalent circuit, amorphous phase morphology can be represented as a continuous or discontinuous second phase.[78–80] According to the continuous second phase model, the disruption due to the thin amorphous layer is assumed with the covered grain boundary area depending on the amount, composition, and wetting properties of the amorphous phase. It is important to have a conduction pathway through the intermediate amorphous phase. In this case, the activation energy of the grain boundary should depend on the particular properties of the blocking phase and the composition of the amorphous phase. The grain boundary activation energy is seen to have a large difference between the C3 and C3A3 samples. The reason could be due to a continuous amorphous phase blocking boundary in the Al_2O_3 doped specimen. By taking the thermal conductivity results for C3 and C3A3 into account, the formation of thin amorphous layer at the grain boundary greatly increased the electrical resistivity of the AlN ceramics without affecting the thermal conductivity. Therefore, the electrical resistivity of AlN samples doped with CaF_2 can be controlled and enhanced by the addition of an appropriate amount of Al_2O_3, which enables and controls the formation of a continuous amorphous phase along grain boundaries.

4. Conclusion

In summary, the thermal conductivity of AlN ceramics is seen to be affected by different factors such as synthesis conditions (ex: cooling and heating rate), sintering additives, and the structure and morphology of second phase formed in grain boundaries. The amount and type of additives and morphology of the second phase play a crucial role in determining the thermal conductivity value of AlN. Different characterization techniques such as Raman spectroscopy and AC impedance spectroscopy were employed to correlate the effect of structural and morphological changes with the thermal conductivity values of AlN ceramics. The density and thermal conductivity of AlN were seen to increase with the inclusion of Y_2O_3, Al_2O_3, and CaF_2 additives. By controlling the cooling rate after the sintering, the formation of the second phase and its interactions (interconnected or isolated) can be controlled within the AlN grains. With the addition of 0.1 wt% CaF_2, the density of the AlN specimen reached 3.21 g cm^{-3}, which is nearly the theoretical density of AlN ceramics. In addition to that, the thermal conductivity is seen to increase rapidly with increasing CaF_2 contents and the thermal conductivity shows the highest value of 211 W m^{-1} K^{-1} with the addition of 2 wt% CaF_2. The thermal conductivity of AlN specimens was theoretically calculated employing several models and the results were compared with the experimentally measured values. A relationship between the broadening of Raman line width and the thermal conductivity of AlN grains calculated from bulk thermal conductivity of AlN was obtained. AC impedance studies on $CaF_2-Al_2O_3$ added AlN samples revealed that the formation of thin amorphous layer at the grain boundaries greatly enhanced the electrical resistivity of the AlN ceramics without an affecting the thermal conductivity.

Received: February 19, 2014
Final Version: February 26, 2014

[1] G. K. Chan, R. E. Jones, *Phys. Rev.* **1962**, *126*, 2055.
[2] T. Mattila, R. M. Nieminen, *Phys. Rev. B* **1996**, *55*, 9571.
[3] H. Ibach, H. Luth, *Solid-State Physics: An Introduction to Principles of Materials Science*, Springer, Aachen, Germany **2009**.
[4] C. Kittel, H. Kroemer, *Thermal Physics*, W. H. Freeman and Company, New York, USA **1980**.
[5] D. D. L. Chung, *Appl. Therm. Eng.* **2001**, *21*, 1593.
[6] A. L. Geiger, M. Jacson, *Adv. Mater. Proc.* **1989**, *136*, 6.
[7] L. H. Sinh, J. M. Hong, B. T. Son, N. N. Trung, J. Y. Bae, *Polym. Compos.* **2012**, *33*, 2140.
[8] C.E. Sroog, *Prog. Polvm. Sci.* **1991**, *2*, 521.
[9] T. J. Mroz, *Ceram. Bull.* **1992**, *1*, 82.
[10] L. M. Sheppard, *Ceram. Bull.* **1990**, *29*, l80l.
[11] M. P. Borom, G. A. Slack, J. W. Szymaszek, *Am. Ceram. Soc. Bull.* **1972**, *51*, 852.
[12] G. A. Slack, R. A. Tanzilii, R. O. Pohl, J. W. Vander Sonde, *J. Phys. Chem. Solids* **1987**, *48*, 641.
[13] T. B. Jackson, A. V. Virkar, K. L. More, R. B. Dinwiddie, Jr., R. A. Cutler, *J. Am. Ceram. Soc.* **1997**, *80*, 142135.
[14] B. E. Belkerk, A. Soussou, M. Carette, M. A. Djouadi, Y. Scudeller, *Appl. Phys. Lett.* **2012**, *101*, 151908.
[15] L. Wei, P. K. Kuo, R. L. Thomas, T. R. Anthony, W. F. Banholzer, *Phys. Rev. Lett.* **1993**, *70*, 3764.
[16] L. Lindsay, D. A. Broido, T. L. Reinecke, *Phys. Rev. Lett.* **2013**, *111*, 025901.
[17] J. Pastrnak, L. Roskokova, *Phys. Stat. Sol.* **1966**, *14*, K5.
[18] J. Edwards, K. Kawabe, G. Stevens, R. H. Tredgold, *Solid State Commun.* **1965**, *5*, 99.
[19] A. K. Solanki, A. Kashyap, T. Nautiyal, S. Auluch, M. A. Khan, *Solid State Commun.* **1995**, *94*, 1009.

DOI: 10.1002/adem.201400078

[20] M. Gadenne, J. Plon, P. Gadenne, *Thin Solid Films* **1998**, *333*, 251.
[21] H. Schulz, K. H. Thiemann, *Solid State Commun.* **1977**, *23*, 815.
[22] A. V. Virkar, *J. Am. Cerum. Soc.* **1989**, *72*, 2031.
[23] S. Ruckmich, *J. Eur. Ceram. Soc.* **1991**, *7*, 335.
[24] Y. Baik, R. A. L. Drew, in *Advanced Ceramic Materials*, Vol. *122–124* (Ed: H. Mostaghaci), Trans Tech Publications, Switzerland **1996**, pp. 553–570.
[25] K. Komeya, A. Tsuge, H. Inoue, H. Ohta, *J. Mater. Sci. Lett.* **1982**, *1*, 1325.
[26] K. Komeya, H. Inoue, H. Ohta, *Yogyo-Kyokai-Shi89* **1981**, *6*, 330.
[27] W.-J. Kim, D. K. Kim, C. H. Kim, *J. Mater. Synth. Process.* **1995**, *3*, 39.
[28] H. K. Lee, D. K. Kim, *J. Am. Ceram. Soc.* **2010**, *93*, 2167.
[29] H. K. Lee, H. M. Lee, D. K. Kim, *J. Am. Ceram. Soc.* **2013**, *97*, 805.
[30] A. V. Virkar, T. B. Jackson, R. A. Cutler, *J. Am. Ceram. Soc.* **1987**, *72*, 2031.
[31] Y. Kurokawa, K. Utsumi, H. Takamizawa, *J. Am. Ceram. Soc.* **1988**, *71*, 588.
[32] W.-J. Kim, Y. T. Moon, D. K. Kim, H.-W. Lee, C. H. Kim, *J. Mater. Sci. Lett.* **1994**, *13*, 1349.
[33] K. Watari, K. Ishizaki, T. Hamasaki, T. Huyuki, *J. Ceram. Soc. Jpn.* **1988**, *96*, 1066.
[34] Y. Iwamoto, A. Kuibira, I. Sugiura, J. Tsubaki, *J. Ceram. Soc. Jpn.* **1992**, *100*, 652.
[35] R. Zahneisen, C. Russel, *J. Mater. Sci.* **1993**, *28*, 870.
[36] S. G. Malghan, P. S. Wang, A. Sivakumar, in *Forming Science and Technology for Ceramics* (Ed: M. J. Cima) American Ceramic Society, Westerville, OH **1992**, pp. 31–37.
[37] N. S. VanDamme, S. M. Richard, S. R. Winzer, *J. Am. Ceram. Soc.* **1989**, *72*, 1409.
[38] A. K. Garg, L. C. De Jonghe, *J. Mater. Res.* **1990**, *5*, 136.
[39] J.-S. Kim, H. Schubert, G. Petzow, *J. Eur. Ceram. Soc.* **1989**, *5*, 311.
[40] C.-M. Wang, F. L. Riley, *J. Eur. Ceram. Soc.* **1992**, *10*, 83.
[41] P. Cortesi, H. K. Bowen, *Ceram. Int.* **1989**, *15*, 173.
[42] E. Liden, M. persson, E. Carlstrom, R. Carlsson, *J. Am. Ceram. Soc.* **1991**, *74*, 1335.
[43] T. Garino, *J. Am. Ceram. Soc.* **1992**, *75*, 514.
[44] P. Bowen, J. G. Highfield, A. Mocellin, T. A. Ring, *J. Am. Ceram. Soc.* **1990**, *73*, 724.
[45] W. D. Kingery, H. K. Bowen, D. R. Uhlmann, in *Introduction to Ceramics, second ed.*, Wiley, New York **1976**.
[46] J. H. Enloe, R. W. Rice, J. W. Lau, R. Kumar, S. Y. Lee, *J. Am. Ceram. Soc.* **1991**, *74*, 2214.
[47] M. Fujimoto, S. Ueda, *J. Ceram. Soc. Jpn.* **1988**, *12*, 1119.
[48] R.-R. Lee, *J. Am. Ceram. Soc.* **1991**, *74*, 2242.
[49] T. Yagi, K. Shinozaki, N. Mizutani, M. Kato, Y. Sawada, *J. Ceram. Soc. Jpn.* **1989**, *97*, 1372.
[50] H. Buhr, G. Muller, *J. Eur. Ceram. Soc.* **1993**, *12*, 271.
[51] T. A. Guiton, J. E. Volmering, K. K. Killinger, *Res. Soc. Symp. Proc.* **1992**, *271*, 851.
[52] P. S. Baranda, A. K. Knudsen, E. Ruh, *J. Am. Ceram. Soc.* **1994**, *77*, 1846.
[53] P. J. Wray, *ACta. Metall.* **1976**, *24*, 125.
[54] L. E. Murr, *Interfacial Phenomena in Metals and Alloys*, Addison-Wesley, New York **1975**.
[55] D. R. Clarke, in *Ceramic Microstructures: Role of Interfaces* (Eds: J. A. Park, A. G. Evans) Plenum Press, New York **1987**.
[56] J. Francl, W. D. Kingery, *J. Am. Ceram. Soc.* **1954**, *37*, 99.
[57] W.-J. Kim, D. K. Kim, C. H. Kim, *J. Am. Ceram. Soc.* **1996**, *79*, 1066.
[58] H. Nakano, K. Watari, K. Urabe, *J. Eur. Ceram. Soc.* **2003**, *23*, 1761.
[59] E. Hagen, Y. Yu, T. Grande, R. Hoier, M. A. Einarsrud, **2002**, *85*, 2971.
[60] Y. C. Liu, H. P. Zhou, L. Qiao, Y. Wu, *J. Mater. Sci. Lett.* **1999**, *18*, 703.
[61] W. J. Parker, R. J. Jenkins, C. P. Butler, G. L. Abbott, *J. Appl. Phys.* **1961**, *32*, 1679.
[62] Q. L. Hu, T. Noda, H. Tanigawa, T. Yoneoka, S. Tanaka, *Nucl. Instrum. Methods Phys. Res. Sect. B* **2002**, *191*, 536.
[63] T. Mattila, R. M. Nieminen, *Phys. Rev. B* **1996**, *54*, 16676.
[64] L. A. Falkovsky, J. M. Bluet, J. Camassel, *Phys. Rev. B* **1998**, *57*, 11283.
[65] V. Lughi, D. R. Clarke, *Appl. Phys. Lett.* **2006**, *89*, 241911.
[66] L. Bergman, D. Alexson, P. L. Murphy, R. J. Nemanich, M. Dutta, M. A. Stroscio, C. Balkas, H. Shin, R. F. Davis, *Phys. Rev. B* **1999**, *59*, 12977.
[67] E. F. McCullen, J. S. Thakur, Y. V. Danylyuk, G. W. Auner, L. W. Rosenberger, *J. Appl. Phys.* **2008**, *103*, 063504.
[68] L. E. McNeil, M. Grimsditch, R. H. French, *J. Am. Ceram. Soc.* **1993**, *76*, 1132.
[69] G. A. Slack, *J. Phys. Chem. Solids* **1973**, *34*, 321.
[70] J. H. Harris, R. A. Youngman, R. G. Teller, *J. Mater. Res.* **1990**, *5*, 1763.
[71] M. Kuball, J. M. Hayes, Y. Shi, J. H. Edgar, *Appl. Phys. Lett.* **2000**, *77*, 1958.
[72] P. G. Klemens, *Physica B* **2002**, *316*, 413.
[73] M. U. Cohen, *Rev. Sci. Instrum.* **1935**, *6*, 68.
[74] T. Kusunose, T. Sekino, K. Niihara, *Acta Mater.* **2007**, *55*, 6170.
[75] J. Yoshikawa, Y. Katsuda, N. Yamada, C. Ihara, M. Masuda, H. Sakai, *J. Am. Ceram. Soc.* **2005**, *88*, 3501.
[76] E. Hagen, Y. Yu, T. Grande, R. Hoier, M. A. Einarsrud, *J. Am. Ceram. Soc.* **2002**, *85*, 2971.
[77] H. Nakano, K. Watari, K. Urabe, *J. Eur. Ceram. Soc.* **2003**, *23*, 1761.
[78] S. P. S. Badwal, *Solid State Ionics* **1995**, *76*, 67.
[79] S. P. S. Badwal, A. E. Hughes, *J. Eur. Ceram. Soc.* **1992**, *10*, 115.
[80] S. P. S. Badwal, S. Rajendran, *Solid State Ionics* **1994**, *70–71*, 83.